frontiers in Materials

ORIGINAL RESEARCH
published: 07 August 2020
doi: 10.3389/fmats.2020.00263

Improving Cyclic Stability of $LiMn_2O_4$/Graphite Battery Under Elevated Temperature by Using 1, 3-Propane Sultone as Electrolyte Additive

Xinxi Li[1], Long Liu[1], Shumin Li[2], Lin Guo[3†], Bin Li[1,3] and Guoqing Zhang[1]**

[1] School of Materials and Energy, Guangdong University of Technology, Guangzhou, China, [2] School of Chemistry and Environment, South China Normal University, Guangzhou, China, [3] School of Chemistry and Materials Engineering, Huizhou University, Huizhou, China

OPEN ACCESS

Edited by:
Federico Cesano,
University of Turin, Italy

Reviewed by:
Xianwen Wu,
Jishou University, China
Renheng Wang,
Shenzhen University, China
Şaban Patat,
Erciyes University, Turkey

***Correspondence:**
Bin Li
lib120@163.com
Guoqing Zhang
pdzgq008@126.com

†Present address:
Lin Guo,
Guangdong Guangxin Holdings Group Ltd., Guangzhou, China

Specialty section:
This article was submitted to Energy Materials, a section of the journal Frontiers in Materials

Received: 26 December 2019
Accepted: 17 July 2020
Published: 07 August 2020

Citation:
Li X, Liu L, Li S, Guo L, Li B and Zhang G (2020) Improving Cyclic Stability of $LiMn_2O_4$/Graphite Battery Under Elevated Temperature by Using 1, 3-Propane Sultone as Electrolyte Additive. Front. Mater. 7:263. doi: 10.3389/fmats.2020.00263

Spinel lithium manganese oxide ($LiMn_2O_4$) based Li-ion battery (LIB) is attractive for hybrid/full electric vehicles because of its abundant resources and easy preparation. However, operation under an elevated temperature could cause severe capacity fading of the spinel cathodes. In this work, 1, 3-propane sultone (PS) is investigated as an electrolyte additive for improving the cyclability of the $LiMn_2O_4$/graphite LIB at elevated temperature. The charge and discharge measurement proves that PS can significantly enhance the cyclability of 053048-type $LiMn_2O_4$/graphite pouch cell at 60°C. Compared to the cell without additive, the capacity retention of the cell using electrolyte with 5% PS increases from 52 to 71% after 180 cycles. The improved cyclability is attributable to the modification of the solid electrolyte interface (SEI) on both positive and negative sides of the $LiMn_2O_4$/graphite cell by PS, which effectively prevents anode and cathode from structural breakdown and inhibits the electrolyte decomposition.

Keywords: 1, 3-propane sultone, solid electrolyte interphase, graphite anode, spinel cathode, lithium ion battery

INTRODUCTION

Li-ion battery (LIB) is successfully applied in portable electronic equipment and is scaled up for hybrid/full electric vehicles and grid storage for renewable energy sources (Cheng et al., 2017; Yu et al., 2020). Spinel lithium manganese oxide ($LiMn_2O_4$) is an ideal material for LIB owing to its superior properties, such as low cost, high operating voltage, good safety, and low toxicity. However, $LiMn_2O_4$ is not widely utilized in LIB commercialization due to its poor cycling performance, especially at high temperature over 55°C (Huang et al., 2018; Hai et al., 2019). Generally, the poor cycling performance is arised from the irreversible crystal phase transition (Jahn–Teller distortion) and oxygen deficiency (Xie et al., 2019), and more importantly, manganese (Mn) ion dissolving into the electrolyte and subsequently deposited on the graphite anode, which degrades the solid electrolyte interphase (SEI) on the electrode surface or deteriorates the graphite structure (Ryou et al., 2010; Liao et al., 2017; Flamme et al., 2020).

Many methods were reported to effectively improve the electrochemical performance of the $LiMn_2O_4$ cells, such as element partial substitutions (Ding et al., 2011; Piao et al., 2018) and

surface coatings (Cao et al., 2018; Li et al., 2018; Zhang et al., 2018). However, alternatives and surface coatings usually cause reversible capacity loss and involve high cost manufacture. The use of surface film-forming electrolyte additive is an effective and facile method to enhance the electrochemical behavior of lithium ion battery. This method cannot only modify the SEI layers on electrodes and prevent the dissolution/deposition of transition metal, but also can inhibit the electrolyte decomposition during the cycling.

Various SEI-film forming additives have been used for enhancing the high temperature stability of the $LiMn_2O_4$-based cells, including sulfur-containing compounds such as methylene methanedisulfonate (Zuo et al., 2014), prop-1-ene-1, 3-sultone (Li Y. et al., 2013), P-toluenesulfonyl isocyanate (Wang et al., 2015), 3, 3′–sulfonyldipropionitrile (Huang et al., 2015), and butyl sultone (Xu et al., 2007). The sulfur-containing substances generated from the additives decomposition can deactivate many catalysts (Czekaj et al., 2011). It helps to build protective surface film on the electrode and suppress decomposition of the electrolyte, which leads to the improved performance of the cell. 1, 3-propane sultone (PS) is one of the most used additives in LIBs (Guo et al., 2008). It has been used as an electrolyte additive in $LiMn_2O_4$-based battery to improve the thermal storage performance. The improvement can be ascribed to its suppression of solvent co-intercalating into graphite anode (Xu et al., 2009).

Although PS has been applied as suppress propylene carbonate (PC) co-intercalation co-solvent and additive to improve the thermal storage performance in $LiMn_2O_4$/graphite cell, the behavior of PS on the cathode reactions, modification of the anode SEI, and thermal cyclability of the cell have not been clearly investigated. Herein, we present a study focused on morphology and structure of the cathode and anode SEI films by using PS as an electrolyte additive in $LiMn_2O_4$/graphite cell. The effect of PS on the cell cyclability at high operating temperature was investigated and the morphologies and chemical compositions of the surface films of the cycled electrodes were also presented.

EXPERIMENTAL

The $LiMn_2O_4$ electrode was prepared by coating a mixture of 90 wt.% $LiMn_2O_4$ (Hunan Reshine New Material Co., Ltd.), 5 wt.% of super-p (MMM carbon, Belgium), and 5 wt.% of polyvinylidene difluoride (PVDF, Shanghai Ofluorine Chemical Technology Co., Ltd.) binder on an aluminum current collect (thickness was 16 um). The active material loading of the $LiMn_2O_4$ electrode was 340 g m^{-2} and the thickness was about 179 um. The graphite electrode was obtained by coating a mixture 95 wt.% of graphite (BTR Battery Materials Co., Ltd.), 1 wt.% of super-p, 2 wt.% carboxymethyl cellulose, and 2 wt.% of styrene butadiene rubber in deionized water on a copper foil (thickness was 8 um). The graphite material loading of the electrode was 155 g m^{-2} and the thickness was about 165 um. The full cells (053048-type) were assembled in an argon-filled dry glove box (Mbraun Unilab MB20, water and oxygen contents were lower than 0.1 ppm) with the $LiMn_2O_4$ electrode as positive electrodes (P) and graphite electrode as negative electrodes (N). The loading weight of the active material for $LiMn_2O_4$/graphite cells was controlled to the specific capacity of N/P = 1.15 (the specific capacity of N and P were 340 and 135 mA h g^{-1} for graphite and $LiMn_2O_4$, respectively). The design capacity of the punch cell was 500 mAh. The separator was a Celgard 2400 membrane. The electrolyte was composed of 1.0 M $LiPF_6$ - ethylene carbonate (EC) / ethyl methyl carbonate (EMC) with the volume ratio of 1:2 (Guangzhou Tinci Materials Technology Co. Ltd, China). 1, 3-propane sultone (PS) was purchased from Aladdin (purity: >99%). The amount of electrolyte used in the pouch cell was controlled to 2.8 g Ah^{-1}.

The electrochemical performance test of the full cell was performed using CT-4008-5V6A-S1 test system (NEWARE, Shenzhen, China) between 2.75 and 4.20 V at room temperature and 60°C, respectively. Five cells were tested with each electrolyte and the reported charge/discharge results are the average values of top three cells. The thickness of cells was tested by a micrometer caliper (Cal PRO IP67, SYLVAC, Swiss). The formula for calculating the swell value of the $LiMn_2O_4$/graphite battery is as follows:

$$\text{Swellvalue}(\%) = (T - T_0)/T_0 \times 100.$$

where T_0 and T are the thickness of the $LiMn_2O_4$/graphite cell before and after 180 cycles at 60°C, respectively.

The internal resistance of cells was measured by resistance meter (HK3561, Meifu, Shenzhen) when the cells cooled down to the room temperature. The formula for calculating the internal resistance rate of the $LiMn_2O_4$/graphite battery is as follows:

Internal resistance rate (%) = $(R\text{-}R_0)/R_0 \times 100$.

where R_0 and R are the internal resistance of the $LiMn_2O_4$/graphite cell before and after 180 cycles at 60°C, respectively.

Conductivity of the electrolyte solutions was measured using a Model DDS-307 conductometer (Shanghai Precision Scientific Instrument Co., Ltd., China). The linear sweep voltammetry (LSV) was performed in Li/Pt cell on Solartron-1408 instrument (England) at a scan rate of 0.2 mV s^{-1} in voltage range of open circuit potential to 5.0 V (vs. Li^+/Li). Cyclic voltammetry of Li/graphite cell was performed on Solartron-1470 instrument (England) in the potential range of 0.01–2.5 V (vs. Li^+/Li) at a scanning rate of 0.2 mV s^{-1}. The diameter and the thickness of Li disk were 15.6 and 0.2 mm, respectively. The graphite and $LiMn_2O_4$ electrodes were disassembled from the full cells and washed with dimethyl carbonate solvent 3 times to remove residual electrolytes. The rinsed electrodes were kept in an antechamber of the glovebox to remove the solvent before conducting surface characterization. The morphology and structure of the electrodes were obtained by a scanning electron microscope (SEM, JEOL JSM-6380) and a transmission electron microscope (TEM, JEOL JEM-2100HR). X-ray diffractometer (XRD, Rigaku Ultima IV, Japan) was used to investigate the crystal structure of the electrode. The chemical composition on the surface of the electrodes was analyzed by X-ray photoelectron spectroscopy (XPS, Kratos Axis Ultra DLD) with Al Ka line ($h\upsilon$ = 1486.6 eV) as a radiation exciting source. X-ray analysis

area for the surface was ~500 × 500 um. Pressure in the analytical chamber during spectral acquisition was less than 5×10^{-9} Torr. Pass energy for survey and detail spectra (to calculate composition) was 80 eV. The take-off angle (the angle between the sample normal and the input axis of the energy analyzer) was 0°, and the input lens was operated in hybrid mode (0° take-off angle = around 100 Å sampling depth). The binding energy was calibrated based on the C 1s level at 284.3 eV (C-C).

RESULTS AND DISCUSSION

Figure 1 depicts the cycling behavior of $LiMn_2O_4$/graphite pouch full-cells without and with variable concentrations of 1, 3-propane sultone (PS) at room temperature at a current of 500 mA. As shown in **Figure 1A**, the reversible capacity of the $LiMn_2O_4$/graphite cell without additive is only 430 mAh in the first cycle, which indicates a large amount of irreversible lithium consumption during charging owing to the decomposition of electrolyte on the anode surface. When PS additive is applied in the electrolyte, the discharge capacities increased. The first cycle capacity of the cells with 3, 5, and 7 wt.% PS addition in the electrolyte are 474, 497, and 467 mAh, respectively. Obviously, when the concentration of PS is 5 wt.%, a most effective SEI film was formed on the electrodes. The SEI film cannot only suppress the electrolyte decomposition but also can benefit the lithium insertion/de-insertion during the cycling. However, the discharge capacity decreased when the PS concentration is higher than 5 wt.%. This phenomenon suggests that excess PS might lead to the formation of a thicker SEI film on the electrode which would hinder the transport of Li^+ in the cells.

Figure 2 shows the cycling performances of $LiMn_2O_4$/graphite cells using the electrolyte without and with various concentrations of PS at 60°C. Before the cycling at high temperature, all the cells were cycling for three times under room temperature at 1C (500 mA). In the cell with additive-free electrolyte, the capacity fading becomes severe during the cycling, as shown in **Figure 2A**. The reversible capacity of the cell using the electrolyte without additive displays about 48% capacity loss at the 180th cycle (**Figure 2B**). At high temperature (60°C), the decomposition of the electrolyte becomes severe and the $LiMn_2O_4$ suffer destruction, result in the dissolution of Mn ions from spinel into the electrolyte. The Mn ions in the electrolyte can deposit on the graphite side and further catalyze

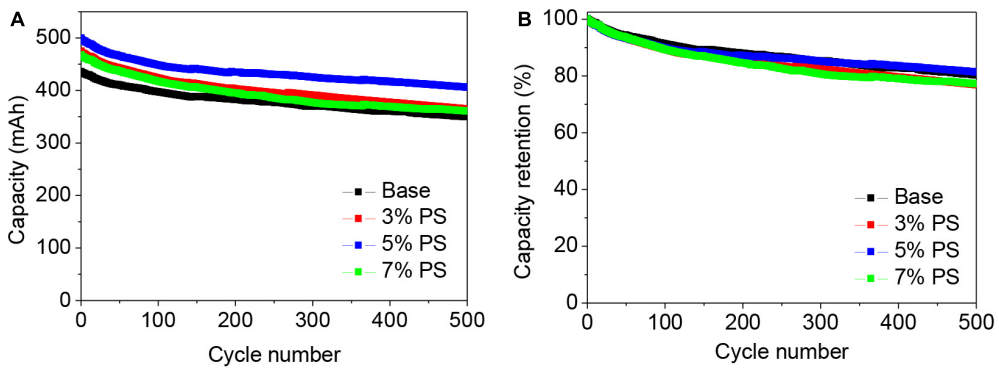

FIGURE 1 | Cyclic stability **(A)** and corresponding capacity retention **(B)** of $LiMn_2O_4$/graphite cells using the electrolyte without (Base), with 3, 5, and with 7 wt.% PS. Charge-discharge rate was 1.0 C in the potential range of 2.75–4.20 V at 25°C.

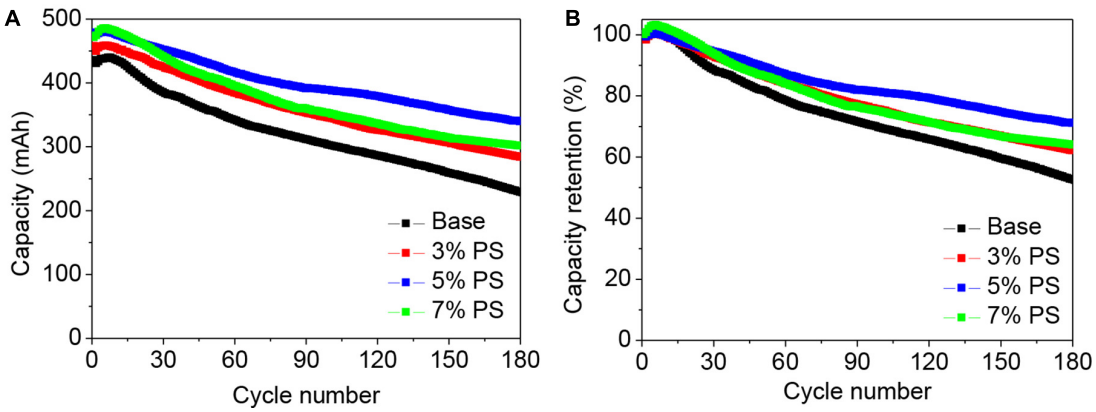

FIGURE 2 | Cycling stability **(A)** and corresponding capacity retention **(B)** of $LiMn_2O_4$/graphite cells using the electrolyte without (Base), with 3, 5, and with 7 wt.% PS. Charge-discharge rate was 1.0 C in the potential range of 2.75–4.20 V at 60°C.

the electrolyte decomposition when the cell was charging, leading to poor cycling performance (Li Y. et al., 2013). In case of the $LiMn_2O_4$/graphite cells using PS, the cycling stabilities are much higher than that of the additive-free cell. The discharge capacity retention of the $LiMn_2O_4$/graphite in the electrolyte using 3, 5, and 7 wt.% PS are 62, 71, and 64%, respectively. This indicates that an excellent SEI film can be formed on graphite with 5 wt.% PS addition. The electrochemical performance of the cell becomes worse when the content of the additive is further increased, which might be related to the over thickness of the SEI film. These results indicate the contribution of PS to the enhanced stability performance of the $LiMn_2O_4$/graphite cells.

The dimensional change and resistance growth of the cells can further confirm that PS can effectively protect the electrolyte from decomposition. **Figure 3** and **Table 1** present the thickness change and resistance growth of the cells before and after 180 cycles at 60°C. Under high temperature, the electrolyte decompositions on both anode and cathode become severe during the cycling, which result in gas generation and structural change of the SEI film and consequently increase the thickness and resistance along the electrodes. The swell value of the cells using electrolyte without, with 3, 5, and 7 wt.% PS are 35.8, 21.3, 6.5, and 7.2%, while the internal resistance rate for those cells are 78.5, 46.4, 31.8, and 38.2%, respectively. Apparently, the electrolyte decomposition in the $LiMn_2O_4$/graphite cells with PS as electrolyte additive can be significantly suppressed at high temperature.

The conductivities of electrolyte without and with different contents of PS were investigated at room temperature. Due to the high melting point of PS (30–33°C), the conductivity of the electrolyte is slightly decreased with the increase content of the additive, as shown in **Table 2**. The conductivity of electrolyte containing 5% PS can reach 8.63 mS cm^{-1}, indicating an insignificant effect on electrolyte conductivity if PS is used within certain limits.

The stability of the electrolyte was also evaluated with linear sweep voltammetry (LSV). **Figure 4** presents the LSV of Pt in the electrolyte with and without PS. The base electrolyte is decomposed at around 4.7 V (vs. Li^+/Li). When adding 5% PS into the electrolyte, oxidation current can be observed at around 4.1 V (vs. Li^+/Li). This behavior implies that the preferential oxidation of PS, suggests PS can form the modified surface film on $LiMn_2O_4$ compared to the base electrolyte.

The reduction behavior of the PS on graphite anode was also investigated by cyclic voltammograms (CV). **Figure 5** shows the CV of graphite electrodes in 1.0 M LiPF6-EC / EMC (1:2) with and without 5% PS. In the electrolyte without additive, a reduction peak located at around 0.5 V (vs. Li^+/Li) can be observed during the first cathodic potential sweep, which is attributed to the reduction of EC in the electrolyte. This reduction peak still appears in the second cycle, although it is smaller than that of the first one, as shown **Figure 5A**. It means the EC-derived SEI film does not completely suppress the further reduction of electrolyte during the second cycle. In the case of the electrolyte with PS, a small reduction peak at around 0.7 V (vs. Li^+/Li) can be observed in the first cycle, and the peak at 0.5 V (vs. Li^+/Li) disappears, as shown in **Figure 5B**. In the second cycle, the reduction peak of PS disappears. These results indicate the preferential reduction of PS and the SEI formed by PS was effective enough to suppress the further decompositions of solvents. It can be noted that the de-intercalation peak of lithium ions swifts to 0.30 V (vs. Li^+/Li) in the second cycle, which is lower than that of the base electrolyte (0.37 V vs. Li^+/Li). This suggests the SEI formed by PS on the first cycle promotes the reaction at the interface and thus leads to higher capacity of the cell than that of the base one.

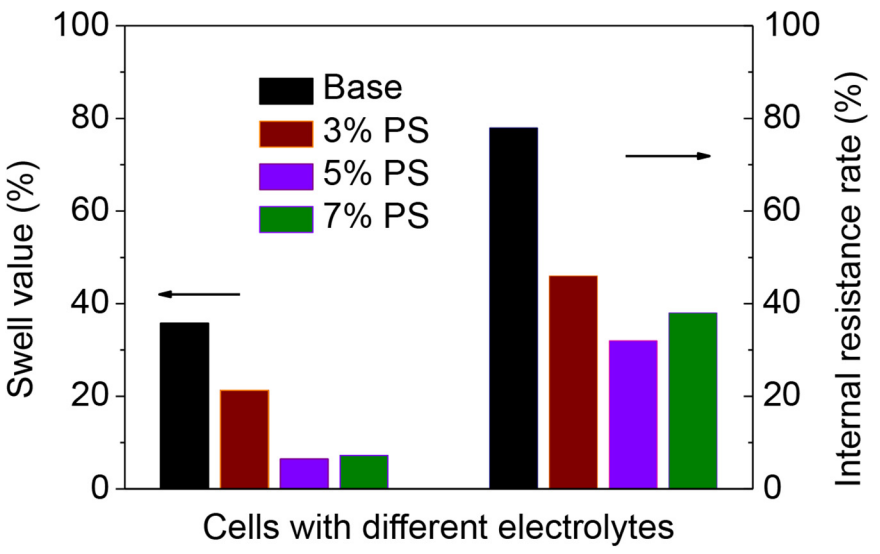

FIGURE 3 | Swell value and internal resistance rate of $LiMn_2O_4$/graphite cells using the electrolyte without (Base) and with variable concentrations of PS after 180 cycles at 60°C.

TABLE 1 | Swell value and internal resistance rate of $LiMn_2O_4$/graphite cells using different electrolytes before and after 180 cycles at 60°C.

Solvent	Additive	Swell value (%)	Internal resistance (%)
EC-EMC(1:2)	Base	35.8	78.2
	3 wt.% PS	21.3	45.9
	5 wt.% PS	6.5	32.1
	7 wt.% PS	7.2	38.4

TABLE 2 | Conductivities of 1.0 M $LiPF_6$ – EC / EMC (1:2) at different content of PS.

Electrolyte	Conductivity (mS cm^{-1})
Base	9.17
3% PS	8.91
5% PS	8.63
7% PS	8.47

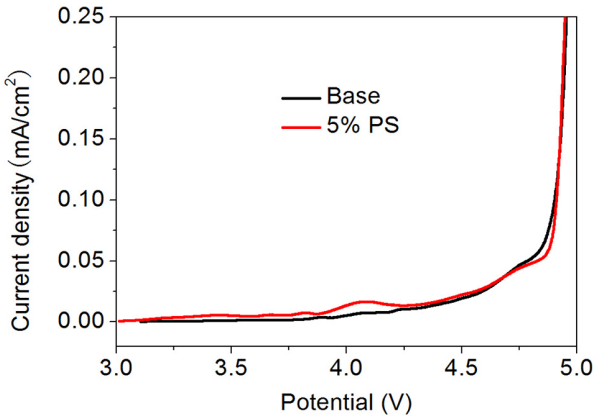

FIGURE 4 | LSV of Pt electrode in 1.0 M $LiPF_6$-EC / EMC (1:2) with and without 5% PS. The area of working electrode was 1.0 cm^2.

To investigate the effect of PS on the improved cyclability of $LiMn_2O_4$/graphite cell at elevated temperature, XRD, SEM, TEM, and XPS measurements were conducted to analyze the morphologies and compositions of the cycled electrode surface films.

The SEM images in **Figure 6** show the surface morphology of the pristine and the graphite electrodes after 180 cycles at 60°C using the electrolyte with and without 5 wt.% PS. The flake-like structure graphite particles with clean surface and sharp edges can be clearly observed in the pristine electrode (**Figures 6a,d**). After cycling in the electrolyte without additive, the electrode surface becomes rough and display a fluffy and thick morphology as shown in **Figures 6b,e**. It suggests that the electrolyte is decomposed and the graphite structure is destroyed. In contrast, the PS electrode continued to display a smooth surface and almost kept relatively similar to original shape of fresh graphite particles after cycling (**Figure 6c**). Moreover, the surface of the graphite particles is evenly covered with a dense surface film. This result indicates that a stable and robust SEI could be formed by the addition of PS, which inhibits further electrolyte decomposition and protects the graphite effectively from exfoliation. The development of sulfur-containing interfaces may allow for the use of electrolytes that are otherwise structural unstable anode materials, such as the Si-based and oxide anode (Wu et al., 2019; Fang et al., 2020).

Figure 7 reveals the SEM and TEM images of the p.ristine $LiMn_2O_4$ and the cathodes cycled with and without PS after 180 cycles. As shown in **Figures 7a,d**, the fresh $LiMn_2O_4$ particles present a typical octahedral spinel shape and the surface are smooth and clean. After cycling in the electrolyte without PS, thick and inhomogeneous deposits can be observed on the spinel particle surface (**Figures 7b,e**), and cracks appear as indicated by the arrow in **Figure 7c**. By contrast, the deposit on the $LiMn_2O_4$ particle with PS additive is uniform

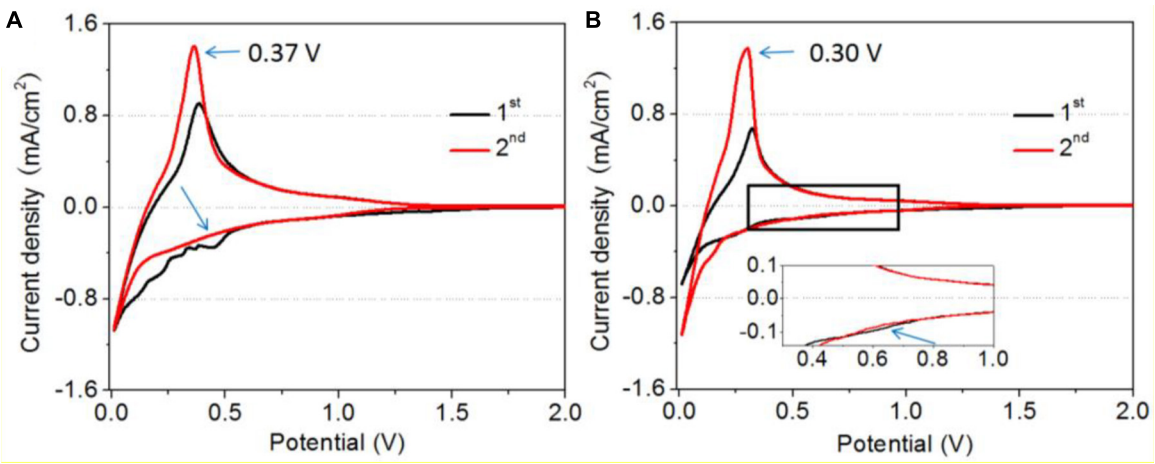

FIGURE 5 | Cyclic voltammograms of graphite electrode in 1.0 M $LiPF_6$-EC / EMC (1:2) without **(A)** and with 5% PS **(B)**. The diameter of graphite electrode was 13.0 mm.

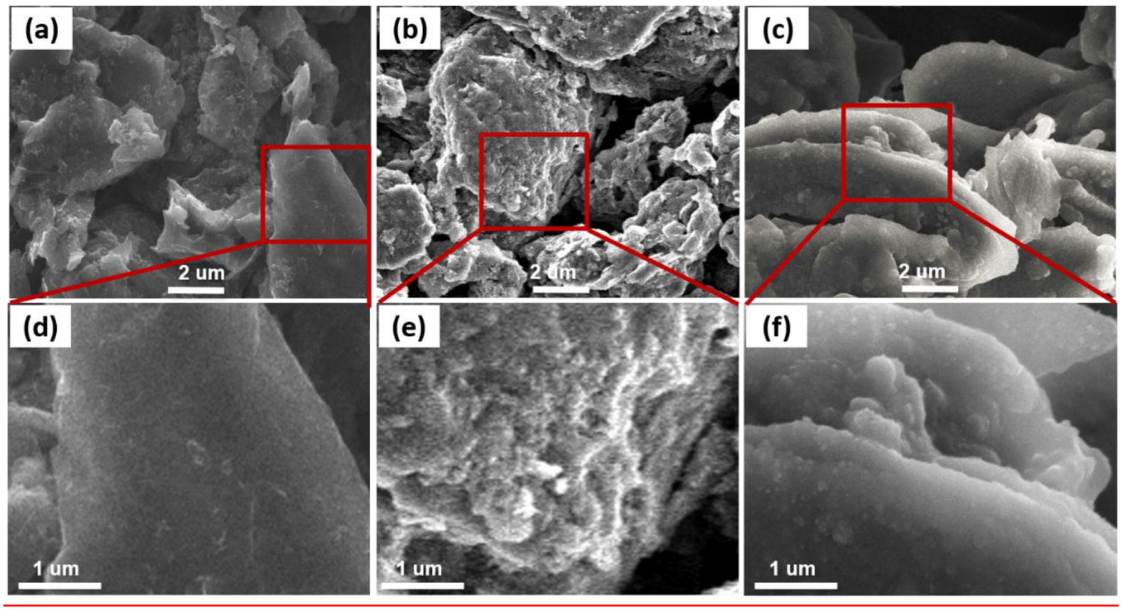

FIGURE 6 | SEM images of pristine graphite anode **(a,d)** and the anodes cycled in the electrolyte without **(b,e)**, with 5 wt.% PS **(c,f)**.

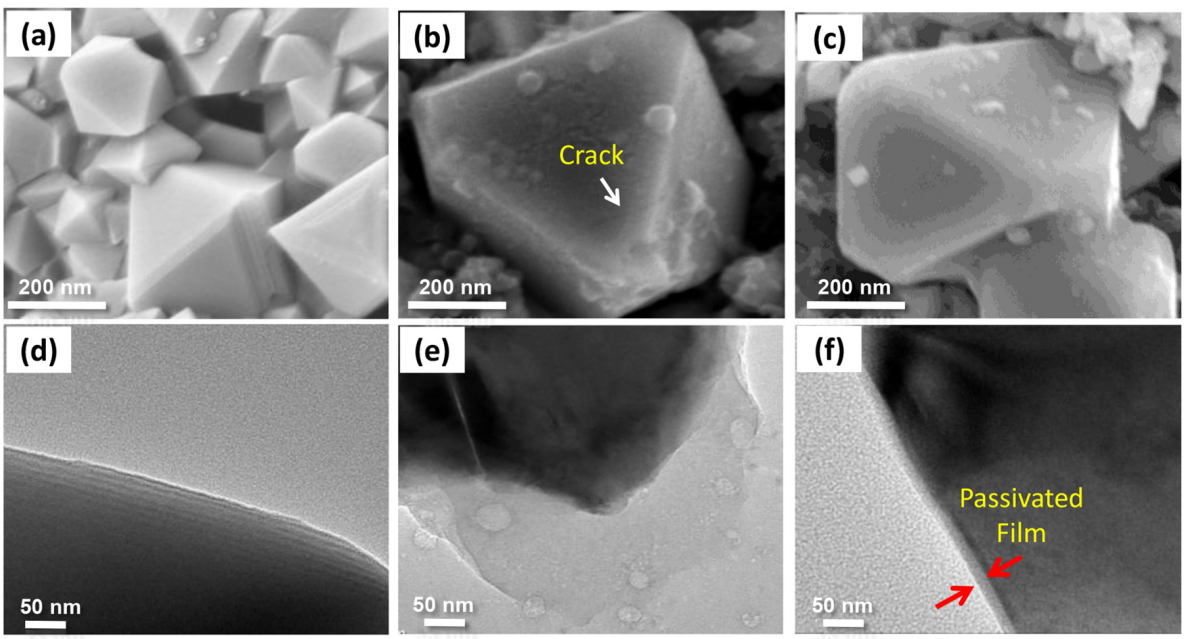

FIGURE 7 | SEM and TEM images for pristine $LiMn_2O_4$ cathode **(a,d)** and the cathode that have been cycled without **(b,e)**, with 5 wt.% PS **(c,f)**.

and thin. The TEM image (**Figure 7f**) displays that the thickness of SEI is around 30 nm. Moreover, the morphology of spinel particle maintains well after cycling. These results indicate that Mn dissolution occurs because of the deterioration of the $LiMn_2O_4$ structure when the cell operated in the base electrolyte. In case of the application of PS as an additive, a protective SEI film can be formed on the cathode surface. This SEI can protect the $LiMn_2O_4$ particles from destruction, inhibits the dissolution of manganese ions from $LiMn_2O_4$ and greatly hinders the continuous decomposition of the electrolyte.

The structural stability of the $LiMn_2O_4$ cycling in the electrolyte with PS was characterized by XRD measurements. As shown in **Figure 8**, all the major diffraction peaks in the pristine electrode and the two cycled $LiMn_2O_4$ electrodes can be indexed to the typical spinel structure for the $LiMn_2O_4$

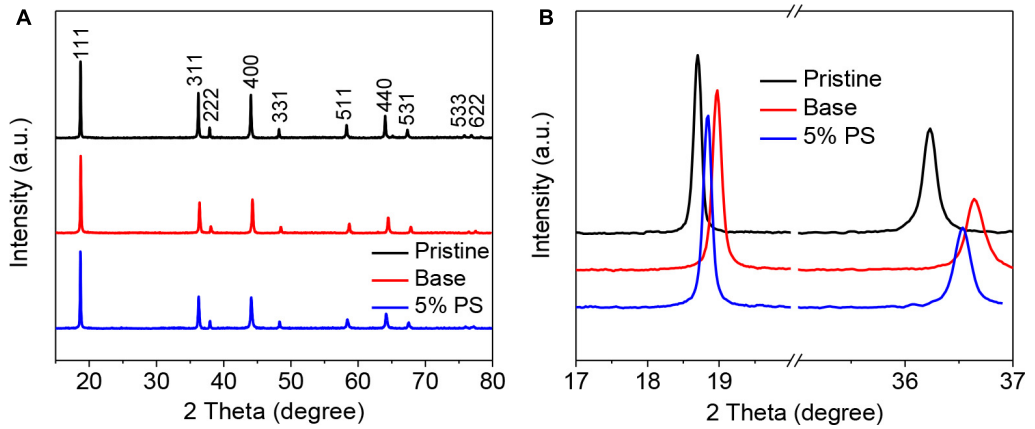

FIGURE 8 | XRD patterns **(A)** and the magnified XRD patterns in the 17–37° 2 Theta interval **(B)** of $LiMn_2O_4$ electrodes before and after cycling in the electrolyte with and without 5 wt.% PS.

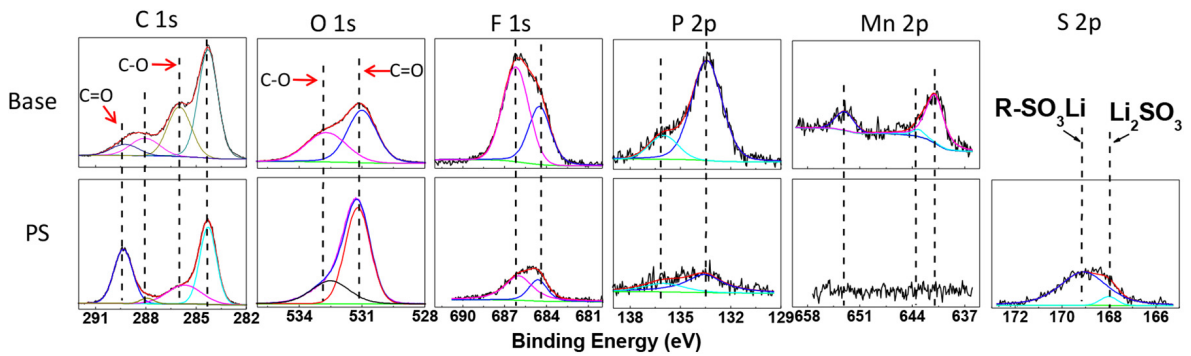

FIGURE 9 | XPS spectra of C 1s, O 1s, F 1s, P 2p, Mn 2p, and S 2p for graphite electrodes after 180 cycles at 60°C in base electrolyte and PS-containing electrolyte.

(JCPDS No. 35-0782). For the $LiMn_2O_4$ cathode cycled with the additive-free electrolyte, the overall intensity of the $LiMn_2O_4$ diffraction peaks is weaker than the pristine electrode, confirming that $LiMn_2O_4$ suffers structural deterioration. This can be ascribed to the severe transition metal (Mn^{3+}) dissolution from the crystal structure that related to the nature of $LiMn_2O_4$ itself (Amatucci et al., 1997; Huang et al., 2018). As shown in **Figure 8B**, the (111) and (311) XRD peaks of electrode cycled without additive shift to higher angles, indicating the crystal lattice shrinkage (Liu et al., 2009). By contrast, the shifting extent for the $LiMn_2O_4$ electrode in the electrolyte with PS is less than that of the electrode without additive, which indicates the SEI formed from PS provides sufficient protection for the crystal structure integrity. This result is in a good agreement with that observed by SEM and TEM. Noted that the shifting still happens while the cell using PS as the electrolyte additive. This might be the reason for the degradation in the cell performance at elevated temperature (as shown in **Figure 2**).

The *ex-situ* XPS spectra have been utilized to investigate the surface compositions of graphite and $LiMn_2O_4$ electrodes. **Figure 9** and **Table 3** reveal the XPS spectra results of graphite anodes after 180 cycles at 60°C. In the C 1s and O 1s spectra, C = O (289.4 eV, 531.2 eV) bond corresponds to lithium carbonates and polycarbonates, while C-O (286.1 and 533.2 eV) bond corresponds to ethers and carbonates (Verma et al., 2010; Zhu et al., 2018). The peak of C = O bond in electrode with PS is much stronger than that of the sample without additive, which indicates that the SEI derived from PS contains more C = O functional groups.

In F 1s spectra, the signals at 684.3 and 686.1 eV are characteristic of lithium fluoride and $Li_xPO_yF_z$ (Dedryvère et al., 2005), respectively. As for P 2p spectra, the binding energy values around 133.3 eV and 136.0 eV are belong to $Li_xPO_yF_z$ and Li_xPF_y (Zheng et al., 2018; Li et al., 2020). These compounds are ascribed to the decomposition products of lithium hexafluorophosphate

TABLE 3 | Element concentrations of the cycled anodes using base electrolyte and PS-containing electrolyte.

	C 1s (%)	O 1s (%)	F 1s (%)	P 2p (%)	Mn 2p (%)	S 2p (%)
Base	46.1	37.7	12.0	2.9	1.3	–
With PS	40.5	53.6	4.4	0.5	–	1.0

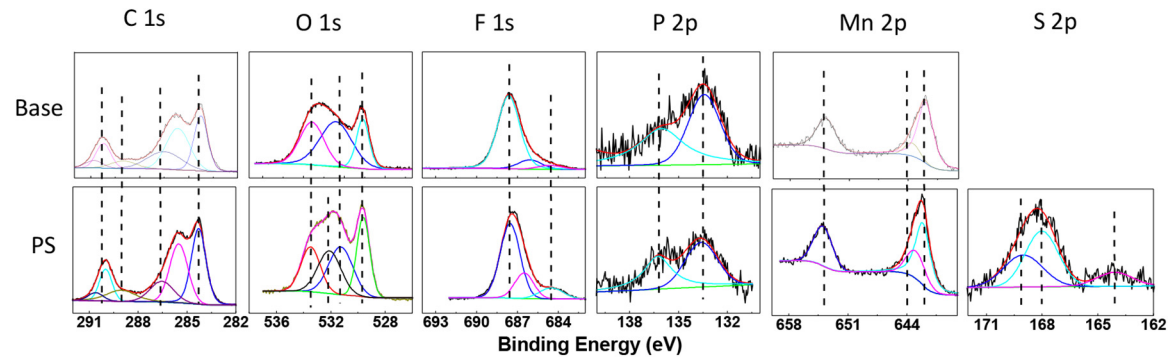

FIGURE 10 | XPS spectra of C 1s, O 1s, F 1s, P 2p, Mn 2p, and S 2p for the $LiMn_2O_4$ electrodes after 180 cycles at 60°C in base electrolyte and PS-containing electrolyte.

in the electrolyte. The concentrations of fluorine and phosphorus discernibly decreased in PS-containing electrolyte, as shown in **Table 3**. Moreover, the anode cycled with PS shows much weaker intensities of lithium fluoride, $Li_xPO_yF_z$ and Li_xPF_y than that of with base electrolyte. It suggests the SEI formed by PS can suppress the decomposition of the electrolyte. It can be noted that the Mn 2p spectrum appears in the graphite electrode, which split into $2p^{3/2}$ and $2p^{1/2}$. The binding energy at 641.1 and 643.1 eV correspond to Mn^{3+} in Mn_2O_3 and Mn^{4+} in MnO_2, while the binding energy at 653.3 eV is attributed to Mn $2p^{1/2}$ (Liu et al., 2016). It indicates that the manganese ions pass through the membrane and deposited on the anode side. On the contrary, the element manganese is hardly detected on the PS graphite electrode, which means the SEI derived from PS can suppress the deposition on the graphite and inhibit the decomposition of the electrolyte. In S 2p spectra, a broad signal around 168–169 eV can be detected in the PS-containing electrolyte, which correspond to Li_2SO_3 and $ROSO_2Li$ (Ota et al., 2003; Li M. et al., 2013), respectively, and this result also clearly indicates that the decomposition products of PS are introduced into SEI.

Figure 10 presents XPS profile of the $LiMn_2O_4$ electrodes in the electrolytes with and without PS after 180 cycles at 60°C, and the related element concentrations are also shown in **Table 4**. The C 1s spectra for $LiMn_2O_4$ cycled in both of the electrolytes mainly contain C from conductive carbon (284.3 eV) and PVDF (285.5 and 290.4 eV) (Verma et al., 2010; Cao et al., 2013), while C-O (285.5 eV), C = O (288.9 eV) and OCO_2 (290.1 eV), respectively from $ROCO_2Li$, ROLi and Li_2CO_3 species that decomposed from the electrolyte (Aurbach et al., 1996). The O1s contains three main peaks for both of the cathodes: Mn_xO_y or $LiMn_2O_4$ (529.5 eV), Li_2CO_3 (531.5 eV), and lithium alkyl carbonates (532.6 eV) (Zuo et al., 2012; Rong et al., 2014). The binding energy at 532 eV in the electrolyte with PS can be related to the decomposition product of PS. The detected peaks at 642.1/643.4 eV and the 653.9 eV correspond to Mn $2p^{3/2}$ and Mn $2p^{1/2}$. Noted that the Mn signals in Mn 2p and Mn–O in O 1s spectra of the PS-containing electrolyte are stronger than that of the electrolyte without additive, suggesting the thin SEI formed by PS on $LiMn_2O_4$ electrode in which more active material can be detected.

The F 1s spectra of **Figure 10** reveal three peaks: PVDF (687.5 eV), $Li_xPO_yF_z$ (686.4 eV), and lithium fluoride (684.6 eV) (Dedryvère et al., 2005). The signals at 133.6 and 135.9 eV in P 2p spectra can be characteristic of $Li_xPO_yF_z$ and Li_xPF_y (Zheng et al., 2018), which are considered to be the decomposition products of the lithium hexafluorophosphate. The peak intensities of $Li_xPO_yF_z$ and Li_xPF_z decreased when the $LiMn_2O_4$ cathode cycled using the electrolyte with PS. It indicates that the SEI derived from PS can reduce the decomposition of lithium hexafluorophosphate on the $LiMn_2O_4$ surface. For the cathode cycled with PS-containing electrolyte, the peak at around 168–169 eV shows the existence of sulfur-containing species (Li_2SO_3 and $ROSO_2Li$) (Ota et al., 2003). This result clearly shows the existence of PS decomposition products in the SEI, and this SEI film can protect the structure of $LiMn_2O_4$ and the dissolution of manganese from spinel particles and inhibit the decomposition of electrolyte.

TABLE 4 | Element concentrations of the cycled cathodes using base electrolyte and PS-containing electrolyte.

	C 1s (%)	O 1s (%)	F 1s (%)	P 2p (%)	Mn 2p (%)	S 2p (%)
Base	47.1	21.2	26.5	1.8	3.4	–
With PS	45.3	23.2	24.8	0.8	4.4	1.5

CONCLUSION

The cycling stability of $LiMn_2O_4$/graphite under elevated temperature can be improved by applying 1, 3-propane sultone (PS) as an electrolyte additive. The enhanced cycling performances are mainly ascribed to the PS-originated solid electrolyte interface (SEI) film on both anode and cathode surface. These SEIs are essential to inhibit the electrolyte decomposition on graphite and $LiMn_2O_4$ electrodes, and protect the spinel structure of $LiMn_2O_4$ from destruction. Moreover, the SEIs can also suppress the dissolution of manganese ions from the cathode and the deposition on the anode.

DATA AVAILABILITY STATEMENT

The raw data supporting the conclusions of this article will be made available by the authors, without undue reservation.

AUTHOR CONTRIBUTIONS

XL and BL conceived and designed the experiments. XL, LL, SL, LG, and BL performed the experiments. XL, LL, and BL analyzed the data. XL and GZ contributed reagents, materials, and analysis tools. XL, LL, BL, and GZ wrote the manuscript. All authors contributed to the article and approved the submitted version.

FUNDING

This work was financially supported by the joint project of the National Natural Science Foundation of China (Grant No. 21875046) and China Postdoctoral Science Foundation (Grant No. 2017M622625).

REFERENCES

Amatucci, C. N., Schmutz, A., Blyr, C., Sigala, A. S., Gozdz, D., Larcher, J. M., et al. (1997). Materials' effects on the elevated and room temperature performance of C/LiMn2O4 Li-ion batteries. *J. Power Sourc.* 69, 11–25.

Aurbach, I., Weissman, A., Schechter, H., and Cohen, H. (1996). X-ray photoelectron spectroscopy studies of lithium surfaces prepared in several important electrolyte solutions. A comparison with previous studies by Fourier transform infrared spectroscopy. *Langmuir* 12, 3991–4007. doi: 10.1021/la9600762

Cao, S., Guo, R., Yan, C., Zhang, J., and Guo, P. (2018). Carbon-coated single-crystalline LiMn2O4 nanowires synthesized by high-temperature solid-state reaction with high capacity for Li-ion battery. *J. Alloys Compd.* 741, 1–6. doi: 10.1016/j.jallcom.2018.01.107

Cao, Y., Li, X., Li, J., Zheng, J., Gao, Y., Gao, X., et al. (2013). Novel phosphamide additive to improve thermal stability of solid electrolyte interphase on graphite anode in lithium-ion batteries. *ACS Appl. Mater. Interf.* 5:11494. doi: 10.1021/am4024884

Cheng, R., Zhang, C. Z., Zhao, T., and Zhang, P. (2017). Toward Safe lithium metal anode in rechargeable batteries: a review. *Chem. Rev.* 117, 10403–10473. doi: 10.1021/acs.chemrev.7b00115

Czekaj, R., Struis, J., Wambach, S., and Biollaz, S. (2011). Sulphur poisoning of Ni catalysts used in the SNG production from biomass: computational studies. *Catal. Today* 176, 429–432. doi: 10.1016/j.cattod.2010.10.078

Dedryveĭre, S., Laruelle, S., Grugeon, L., Gireaud, J.-M., Tarascon, P., and Gonbeau, D. (2005). XPS identification of the organic and inorganic components of the electrode/electrolyte interface formed on a metallic cathode. *J. Electrochem. Soc.* 152, A689–A696.

Ding, J., Xie, G. S., Cao, T. J., Zhu, H. M., Yu, X. B., and Zhao, B. (2011). Enhanced elevated-temperature performance of Al-doped single-crystalline LiMn2O4 nanotubes as cathodes for lithium ion batteries. *J. Phys. Chem. C.* 115, 9821–9825. doi: 10.1021/jp201669x

Fang, C., Miao, H., Mou, W., and Xiao, M. (2020). Facile synthesis of Si@TiO2@rGO composite with sandwich-like nanostructure as superior performance anodes for lithium ion batteries. *J. Alloy Compd.* 818, 152884. doi: 10.1016/j.jallcom.2019.152884

Flamme, D. J., Yeadon, S., Phadke, S., and Anouti, M. (2020). Promising routes to a high Li+ transference number electrolyte for lithium ion batteries. *J. Energy Chem.* 52, 332–342.

Guo, Z., Yin, Z., Tao, X., Li, Z., and Wang, T. (2008). An advanced electrolyte for improving surface characteristics of LiMn2O4 electrode. *J. Power Sourc.* 184, 513–516. doi: 10.1016/j.jpowsour.2008.03.018

Hai, Z., Zhang, H., Liu, L., Liao, P., Fan, Y., Wu, G., et al. (2019). Facile controlled synthesis of spinel limn2o4 porous microspheres as cathode material for lithium ion batteries. *Front. Chem.* 7:437. doi: 10.3389/fchem.2019.00437

Huang, N., Zheng, Y., Pan, W., Wang, G., Fang, M., and Wu, R. (2015). 3, 3'-sulfonyldipropionitrile: a novel additive to improve the high temperature performance of lithium-ion battery. *Electrochim. Acta* 156, 328–335. doi: 10.1016/j.electacta.2015.01.006

Huang, X., Zheng, G., Fang, Y., Pan, W., Wang, R., and Wu, M. (2018). A novel electrolyte additive for improving the interfacial stability of LiMn2O4 cathode lithium-ion batteries at elevated temperature. *RSC Adv.* 8, 38831–38835. doi: 10.1039/c8ra08355j

Li, X., Chen, Y., Liu, Y., and Chen, W. (2018). One-time sintering process to synthesize ZrO2-coated LiMn2O4 materials for lithium-ion batteries. *RSC Adv.* 8, 16753–16761. doi: 10.1039/c8ra01421c

Li, X., Lin, H., Zhou, L., Xing, G., Lan, W., Zhang, J., et al. (2020). Stabilizing the interphasial layer of Ni-rich cathode and graphite anode for lithium ion battery with multifunctional additive. *J. Power Sources* 467, 228343. doi: 10.1016/j.jpowsour.2020.228343

Li, Y., Wang, H., Rong, Y., Wang, J., Liu, L., Xing, M., et al. (2013). A novel electrolyte with the ability to form a solid electrolyte interface on the anode and cathode of a LiMn2O4/graphite battery. *J. Mater. Chem. A* 1, 12954–12961.

Li, M., Xu, B., Li, Y., Liu, L., Yang, W., and Li, S. (2013). Properties of solid electrolyte interphase formed by prop-1-ene-1,3-sultone on graphite anode of Li-ion batteries. *Electrochim. Acta* 105, 1–6. doi: 10.1016/j.electacta.2013.04.142

Liao, H., Li, X., Wang, M., Xu, L., Xing, Y., Liao, X., et al. (2017). Significantly improved cyclability of lithium manganese oxide, simultaneously inhibiting electrochemical and thermal decomposition of the electrolyte by the use of an additive. *RSC Adv.* 7, 46594–46603. doi: 10.1039/c7ra07870f

Liu, Q. C., Zhuang, Y. L., Shi, X. D., Yan, X., Zhao, N., and Chen, X. B. (2016). Tertiary butyl hydroquinone as a novel additive for SEI film formation in lithium-ion batteries. *RSC Adv.* 6, 42885–42891. doi: 10.1039/c6ra04839k

Liu, Y. J., Li, X. H., Guo, H. J., Wang, Z. X., Hu, Q. Y., Peng, W. J., et al. (2009). Electrochemical performance and capacity fading reason of LiMn2O4/graphite batteries stored at room temperature. *J. Power Sour.* 189, 721–725. doi: 10.1016/j.jpowsour.2008.08.044

Ota, T., Akai, H., Namita, S., Yamaguchi, M., and Nomura, M. (2003). XAFS and TOF-SIMS analysis of SEI layers on electrodes. *J. Power Sourc.* 119–121, 567–571. doi: 10.1016/s0378-7753(03)00291-x

Piao, S.-Y., Duan, X.-J., Lin, X.-S., Tao, Y.-S., Xu, A.-M., Cao, L.-J., et al. (2018). Surface Zn doped LiMn2O4 for an improved high temperature performance. *Wan. Chem. Commun.* 54, 5326–5329. doi: 10.1039/c8cc01878b

Rong, M. Q., Xu, L. D., Xing, W. S., and Li, M. (2014). Enhanced cyclability of LiNi0.5*Mn*1.5O4 cathode in carbonate based electrolyte with incorporation of tris(trimethylsilyl)phosphate (TMSP). *J. Power Sourc.* 261, 148–155. doi: 10.1016/j.jpowsour.2014.03.032

Ryou, G.-B., Han, Y. M., Lee, J.-N., Lee, D. J., Lee, Y. O., Yoon, J.-K., et al. (2010). The effects of humidity on the self-discharge properties of Li(Ni1/3Co1/3Mn1/3)O2/graphite and LiCoO2/graphite lithium-ion batteries during storage. *Electrochim. Acta* 55, 2073–2077.

Verma, P., Maire, P., and Novák, P. (2010). A review of the features and analyses of the solid electrolyte interphase in Li-ion batteries. *Electrochim. Acta* 55, 6332–6341. doi: 10.1016/j.electacta.2010.05.072

Wang, R., Li, X., Wang, Z., Guo, H., and Wang, J. (2015). Electrochemical analysis for cycle performance and capacity fading of lithium manganese oxide spinel cathode at elevated temperature using p-toluenesulfonyl isocyanate as electrolyte additive. *Electrochim. Acta* 180, 815–823. doi: 10.1016/j.electacta.2015.09.019

Wu, X., Li, Y., Zhao, S., Zeng, F., Peng, X., Xiang, Y., et al. (2019). Fabrication of F-doped, C-coated NiCo2O4 nanocomposites and its electrochemical performances for lithium-ion batteries. *Solid State Ionics* 334, 48–55. doi: 10.1016/j.ssi.2019.01.039

Xie, R., Jin, Y., and Xiang, L. (2019). Tuning the nanoarea interfacial properties for the improved performance of Li-Rich polycrystalline Li-Mn-O Spinel. *ACS Appl. Mater. Interf.* 11, 14796–14802. doi: 10.1021/acsami.9b01651

Xu, W., Li, B. L., and Lucht, L. (2009). Effect of propane sultone on elevated temperature performance of anode and cathode materials in lithium-ion batteries. *J. Power Sourc.* 193, 804–809. doi: 10.1016/j.jpowsour.2009.03.067

Xu, W. S., Li, X. X., Zuo, J. S., Liu, S., and Xu, X. (2007). Performance improvement of lithium ion battery using PC as a solvent component and BS as an SEI forming additive. *J. Power Sourc.* 174, 705–710. doi: 10.1016/j.jpowsour.2007.06.112

Yu, L., Zhao, Y., Huang, Y., Hu, L., Chen, Y.-B., and He, R. (2020). Progress and perspective of constructing solid electrolyte interphase on stable lithium metal anode. *Front. Mater.* 7:71. doi: 10.3389/fmats.2020.00071

Zhang, J., Su, T., Wang, K., Yuan, C., Chen, S., Liu, T., et al. (2018). Porous polyethylene bundles with enhanced hydrophobicity and pumping oil-recovery ability via skin-peeling. *ACS Sustain. Chem. Eng.* 6, 7890–7901.

Zheng, L., Xing, X., Yang, X., Li, C., Ye, K., Wang, Q., et al. (2018). N-Allyl-N, N-Bis (trimethylsilyl) amine as a novel electrolyte additive to enhance the interfacial stability of a Ni-rich electrode for lithium-ion batteries. *ACS Appl. Mater. Interf.* 10, 16843–16851. doi: 10.1021/acsami.8b00913

Zhu, X., Luo, H., Zhi, Y., Liao, L., Xing, M., Xu, X., et al. (2018). Diethyl (thiophen-2-ylmethyl) phosphonate: a novel multifunctional electrolyte additive for high voltage batteries. *J. Mater. Chem.* 6, 10990–11004. doi: 10.1039/c8ta01236a

Zuo, C., Fan, X., Xiao, J., Liu, J., and Nan, P. (2012). High-voltage performance of LiCoO2/graphite batteries with methylene methanedisulfonate as electrolyte additive. *J. Power Sourc.* 219, 94–99. doi: 10.1016/j.jpowsour.2012.07.026

Zuo, J., Wu, C., Fan, K., Lai, J., Liu, J., and Nan, P. (2014). A novel electrolyte additive for improving the interfacial stability of LiMn2O4 cathode lithium-ion batteries at elevated temperature. *Electrochim. Acta* 130, 778–784.

Conflict of Interest: The authors declare that the research was conducted in the absence of any commercial or financial relationships that could be construed as a potential conflict of interest.